

## Research Article

# Mesoscale Convective Systems in Central Africa: Characteristics of the Associated Seasonal and Diurnal Cycle of Observed Surface Meteorological Parameters

**Stella Songwe Tikeng<sup>1</sup>**, **Wilfried Mba Pokam<sup>1,2</sup>** and **Richard Washington<sup>3</sup>**

<sup>1</sup>Laboratory for Environmental Modelling and Atmospheric Physics (LEMAP), University of Yaounde 1, Yaounde, Cameroon

<sup>2</sup>Department of Physics, Higher Teacher Training College, University of Yaounde 1, Yaounde, Cameroon

<sup>3</sup>Climate Research Lab, School of Geography and the Environment, University of Oxford, Oxford, UK

Correspondence should be addressed to Stella Songwe Tikeng; [stellatikengsongwe@gmail.com](mailto:stellatikengsongwe@gmail.com)

Received 6 July 2023; Revised 15 June 2024; Accepted 1 July 2024

Academic Editor: Mojtaba Nedaei

Copyright © 2024 Stella Songwe Tikeng et al. This is an open access article distributed under the Creative Commons Attribution License, which permits unrestricted use, distribution, and reproduction in any medium, provided the original work is properly cited.

This study examines mesoscale convective systems (MCSs) in relation to 1-min automatic weather station data for 2 years over the city of Yaounde. The focus is on characterising the atmospheric variability associated with MCS activity while distinguishing the days with and without MCS activities. This paper aims to determine the diurnal cycles of occurrence frequencies and percentages of rainfall, relative humidity, dew point temperature, solar radiation, temperature, and wind speed for days with and without MCSs. There are more than 623 MCS events during the study period (over 150 events per rainy season). The link between MCS activity and regional-scale circulation and atmospheric instability is investigated. The diurnal cycle of the number of MCSs shows a maximum in the afternoon (around 1,600–2,200 LT), a morning minimum (around 0700–1,300 LT), and substantial activity during the night. Surface relative humidity is 5% lower on non-MCS days, surface dew point 2% higher on MCS days between 0700 and 1800 hr, and solar radiation higher on MCS days between 0500 and 1000 hr. The percentage of rainfall associated with MCSs can exceed 60% on an annual scale and up to 80% on a seasonal scale. MCS activity is associated with instability in the lower troposphere, and this convective instability is maximal during the peak of the MCS activity.

## 1. Introduction

It has long been known that large-scale, organised convection in the tropics is key to the distribution of rainfall [1, 2]. Mesoscale convective systems (MCSs) are critical to the link between rainfall and the large-scale circulation [3] which includes feedback on atmospheric waves in which convection is embedded [4].

Within Africa, MCSs have been studied in the Sahel [2, 5, 6], Central Africa (CA) [7, 8], as well as Southern Africa [9, 10]. MCSs are responsible for more than 50% of precipitation in almost all regions where the mean annual precipitation exceeds 3 mm/day and for more than 70% of precipitation in CA [11, 12].

MCSs have the advantage of being observable with reasonable spatial and good temporal resolution by geostationary satellites. Their simulation by modern global reanalysis products is severely limited by the difficulties of global products

in resolving tropical MCS dynamics and the fact that tropical MCSs often occur over poorly observed regions [13]. Furthermore, the sensitivity of the performance of the models in reproducing the diurnal cycle of convection to spatial resolution has not yet been fully addressed [14]. Indeed, large-scale models do not always succeed in capturing the phase and amplitude of the diurnal cycle. As a result, establishing the impact of MCSs on surface meteorology is dependent on observational meteorological networks. In CA, there is a dearth of such data along with evidence that the observing system is in decline [15]. It is unsurprising that the vast majority of studies depend on satellites as the key data set for analysis. Understanding the impact of MCSs on specific surface meteorological conditions is not possible with satellites alone.

Meanwhile, there is persuasive evidence that the frequency of severe storms is increasing. Over North tropical Africa, for example, the count of such systems has tripled between 1982

and 2016 [16]. There is also rapid growth in nearly all major cities in Africa [17] with the result that the impact of flash flooding is high and expected to worsen with climate change [18]. On shorter timescales, the forecasting capability of MCSs is poor [19]. This failure of the models is likely related to their poor ability to capture the spatiotemporal pattern of convection development and organisation, due to the small-scale nature of many of the features that contribute to the initiation, development, and organization of convection [20]. The different representation of the MCS in models contributes to the bias between models [21]. A key way to improve model performance is to better describe the multiscale physical processes that govern the activity of MCSs so that models can be assessed against these observed processes. This is particularly important given that what is known about MCSs in CA derives largely from satellite analyses from which meteorological parameters are not available. Improving the understanding of the interaction between MCSs and the local environmental parameters in which rainfall is produced is therefore an important starting point.

Environmental conditions have been shown to be important determinants of MCS activity [3, 22, 23, 24]. Given a combination of moisture, instability, and wind shear, triggering mechanisms such as diurnal heating, convergence zones, or topographic features have all been shown to be important. In CA, an understudied region of Africa [7, 11, 25], the city of Yaounde is a representative location to study propagating MCSs. Yaounde, also known as the city of seven hills, is located in southern Cameroon (in the western part of equatorial Africa), which lies in the rain belt between the cores of two mid-tropospheric jets: the African Easterly Jet of the Southern Hemisphere (AEJ-S) and the African Easterly Jet of the Northern Hemisphere (AEJ-N) [26]. As a result, the region is regularly affected by convective systems, the main consequence of which is an increase in flooding and related disasters [27, 28]. More importantly, Yaounde has an abundance of highlands that can trigger orographic rainfall. The city's proximity to the Atlantic ocean and its location on the westward trajectory of MCSs formed in the East African highlands make it an interesting area to study MCS activity. Yaounde has a bimodal climate regime with the first rainy season during the March–May season and the second during the September–November season [29, 30]. These two rainy seasons have been identified in previous studies as the seasons during which most of the annual precipitation provided by MCSs is recorded in CA (e.g., [7, 22, 25]). These regional-scale studies have also shown that maximum MCS activity is recorded on the continent around 1,500–1,800 TL [25, 31]. However, they did not allow us to assess the interaction between MCSs and local environmental factors. The origin of precipitation associated with MCSs therefore remains to be investigated, as the ability to predict convective (and even stratiform) precipitation depends on an understanding of the evolution and environment of MCSs [22].

Establishing the link between MCSs and precipitation, surface meteorological parameters, regional-scale circulation, and atmospheric instability is the main concern of this paper. We use a rare, high-resolution surface automatic weather

station (AWS) data set from Yaounde, Cameroon, in conjunction with satellite imagery, to study the activity of MCSs, their influence on the diurnal variation of atmospheric parameters, and local precipitation. We also analyse the frequency of occurrence of MCSs, their impact on the stability of the atmosphere, and their links with regional circulation. We demonstrate the merits of connecting satellite-based analysis with high-time resolution surface observations.

The analysis begins with the presentation of the diurnal cycle of MCSs before proceeding to the evaluation of the diurnal cycle of relative humidity, dew point temperature, solar radiation, temperature, and wind speed for dates with and without MCSs. The characteristics of these parameters, together with the satellite-derived MCS diurnal cycle, are then related to the diurnal cycle of rainfall. The paper progresses to the definition of rainfall seasons for 2019 and 2020 from the AWS data before assessing the seasonal characteristics of MCSs and associated rainfall through the diurnal cycle in each of the two rainfall seasons. We end with an assessment of atmospheric thermodynamics and large-scale circulation.

## 2. Data and Methodology

**2.1. Data.** In this work, our study area (Yaounde), corresponding to the black box, is located at 3.51°North and 11.31°East (Figure 1). Both observation and reanalysis data are used to investigate MCSs activity over the region.

The observation data used are provided by the AWS of the Higher Teacher Training College of the University of Yaounde 1. Six parameters are used, namely, rainfall, dew point temperature, relative humidity, surface temperature, solar radiation, and wind speed, to study the atmospheric characteristics at the surface associated to days with and without MCS events. These data are recorded with a resolution of 1-min resolution from 5 February 2019 to 5 February 2021.

As a proxy for observational data, which are very coarse in CA [15, 32, 33], reanalysis datasets are usually used to perform process and climate characterisation [34]. Among these reanalyses, the fifth generation European Reanalysis (ERA5) global dataset, produced by the Copernicus Climate Change Service (C3S) of the European Centre for Medium-Range Weather Forecasts (ECMWF), has shown the best accuracy in representing the climate and weather systems of Central Africa [34, 35]. Thus, in this study the 2019 and 2020 ERA5 hourly specific humidity, temperature, and zonal wind data provided by the Copernicus Climate Change Service [36] are used for the representation of African Easterly Jet (AEJ) and the estimation of equivalent potential temperature. The ERA5 hourly dataset is on a  $0.25^\circ \times 0.25^\circ$  spatial grid with 37 pressure levels from 1,000 to 1 hPa.

### 2.2. Methodology

**2.2.1. MCS Occurrence.** The most commonly used method for the detection and tracking of MCSs is the brightness temperature thresholding detection method. It consists of applying a brightness temperature threshold ( $BT_{\text{threshold}}$ ) to infrared imagery [37]. A convective cell is defined as an area

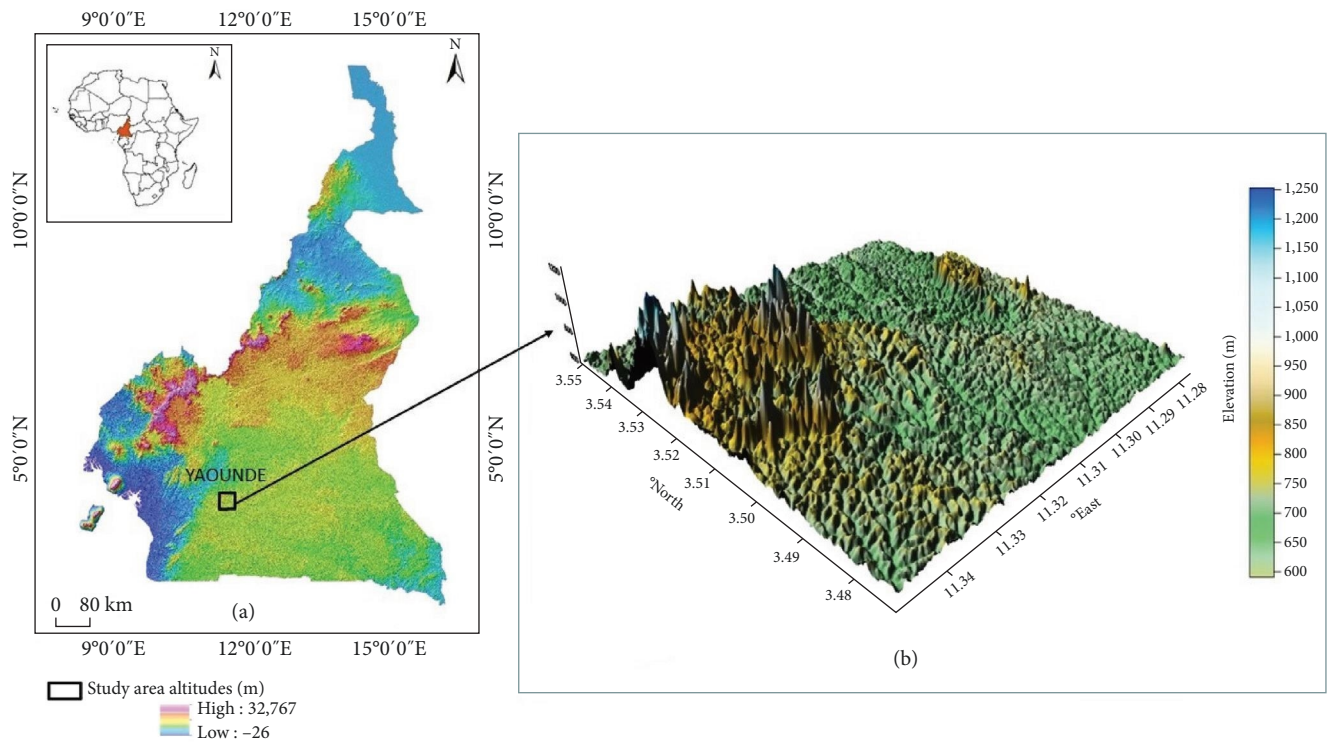


FIGURE 1: Geographical location of (a) Cameroon (in orange on the map of Africa), location of the Yaounde analysis region on the topographic map of Cameroon (a, black box) and (b) 3D digital terrain model (DTM) of the Yaounde site.

of pixels with a brightness temperature less than or equal to  $BT_{\text{threshold}}$  whose size is greater than area coverage thresholds. Several studies have used this method to track MCSs [6, 22, 38, 39, 40, 41, 42, 43]. Mathon and Laurent [6] identified MCSs from Meteosat images in the infrared channel ( $10.5\text{--}12.5\ \mu\text{m}$ ) by applying three temperature thresholds to the infrared imagery. This allowed them to follow MCSs throughout their life cycle. However, techniques based only on the infrared channel tend to overestimate both the spatial extent and the lifetime of convective systems due to the presence of cirrus clouds [39]. The problem is more pronounced in mountain regions like the Tibetan plateau region, where Kukulies et al. [43] applied a brightness temperature threshold criteria indiscriminating between low surface temperatures of high mountain tops and the tops of convective cloud clusters, especially at night during winter.

Due to the latitudinal location of our study area, the use of the brightness temperature threshold criterion alone is acceptable for the detection of MCSs, as the confusion of MCSs with cold mountain top surfaces is not relevant. As for cirrus clouds, they are on average 1,500 m thick [44], compared to 10.0 km for deep convective clouds. It is therefore extremely difficult to identify fine cirrus clouds using IR temperature techniques from satellites [45]. In addition, it has been shown that cirrus clouds are grey body emitters (infrared emittances  $< \sim 0.85$ ) [46], whereas MCSs are black bodies that are easily detectable by infrared radar using a brightness temperature threshold. The cloud clusters in the infrared images used should therefore be mainly MCSs.

In this study, a sample of 623 MCS events were detected at 3-hourly time resolution between 5 February 2019 and 5 February 2021 using the EUMeTrain MapViewer infrared imaging products available online ([https://resources.eumetrain.org/ePort\\_MapViewer/index.html](https://resources.eumetrain.org/ePort_MapViewer/index.html)). All identified MCS cells crossing the geographical coordinates of Yaounde were counted; provided that the cells covered the entire city of Yaounde (which has an area of  $304\text{ km}^2$ ) and its surroundings. EUMeTrain provides a wide range of satellite products, including an infrared channel of  $10.8\ \mu\text{m}$  labelled “Enhanced Infrared 10.8” from Meteosat, which is used in this study. This option uses the brightness temperature thresholding detection method and allows the visualisation of MCSs in the brightness temperature range of 200–240 K. These data are available online since 5 February 2019 and can be viewed at 3-hourly time resolutions.

**2.2.2. Determining the Onset and Cessation of the Rainy Seasons.** We used the analysis method described by Dunning et al. [47] adapted from Liebmann et al. [48] to determine the start and end dates for each of the two rainy seasons over CA and each of the 2 years of the study. This method is divided into two stages.

(1) *Determining the seasonality.* A harmonic analysis is applied to the entire time series to determine whether one or two wet seasons are recorded per year. The amplitudes of the first and second harmonics are calculated. The ratio between the amplitude of the second harmonic and the amplitude of the first harmonic is then used to determine seasonality. A

ratio greater than 1.0 indicates a biannual regime, and a ratio less than 1.0 indicates an annual regime.

(2) *Determining the onset and cessation of biannual regimes.* To determine the period of the year when the wet season occurs, we need to take into account the seasons that extend over the calendar year (from 1 January to 31 December). We calculate the climatological mean rainfall for each day  $Q_i$ , where  $i$  goes from 1 January to 31 December, and the climatological mean daily rainfall  $\bar{Q}$ . From this, we can deduce the climatological cumulative daily rainfall anomaly for day  $d$ ,  $C(d)$ :

$$C(d) = \sum_{i=1}^d Q_i - \bar{Q}, \quad (1)$$

where  $i$  runs from 1st January to day  $d$  for which the calculation applies. The minima/maxima in the curve are detected by identifying the days when  $C(d)$  is lower/higher than the four previous days and lower/higher than the four following days. The minimum days in  $C$  mark the beginning of the wet seasons  $d_{s1}$ ,  $d_{s2}$ , and the maximum days in  $C$  mark the end of the seasons  $d_{e1}$ ,  $d_{e2}$ .

**2.2.3. Calculation of the Frequency of Occurrence of MCSs.** In this study, the annual frequency of occurrence,  $F_{0A}$  (seasonal for season  $i$ ,  $F_{0S}(i)$ ) of MCSs is defined as the ratio of the daily cumulation of MCSs on day  $j$  ( $C_j$ ) to the number of days in the year,  $N$  (the season,  $N_S$ ) and given by Equations (2) and (3).

By calculating the ratio between the daily cumulation of MCSs on day  $j$  ( $C_j$ ) by the number of days in the year,  $N$  (the season,  $N_S$ ), we obtain the annual frequency of occurrence,  $F_{0A}$  (seasonal for season  $i$ ,  $F_{0S}(i)$ ) of MCSs:

$$F_{0A} = \frac{\sum_{j=1}^{31\text{Dec}} C_j}{N} \times 100, \quad (2)$$

$$F_{0S}(i) = \frac{\sum_{j=1}^{N_S} C_j}{N_S} \times 100. \quad (3)$$

The same approach is used to calculate the annual and seasonal 3-hourly frequency of occurrence. The ratio between the 3-hourly cumulation of MCSs for the time step  $k$  chosen on day  $j$  ( $C_{jk}$ ) by the number of days in the year,  $N$  (the season,  $N_S$ ) is obtained as the annual,  $F_{0HA}(k)$  (seasonal,  $F_{0HS}(ik)$ ) 3-hourly frequency of occurrence for the time step  $k$ :

$$F_{0HA}(k) = \frac{\sum_{j=1}^{31\text{Dec}} C_{jk}}{N} \times 100, \quad (4)$$

$$F_{0HS}(ik) = \frac{\sum_{j=1}^{N_S} C_{jk}}{N_S} \times 100. \quad (5)$$

**2.2.4. Calculation of the Percentage of Precipitation Associated with MCSs Activity.** The percentage of rainfall associated with MCS activity is defined as the fraction of rainfall recorded on

days when MCS activity was observed in Yaounde. Therefore, calculating the ratio of the cumulative daily rainfall for each day  $j$  ( $p_j$ ) of MCS activity to the cumulative daily rainfall for each day  $l$  ( $p_l$ ) of the year (season) under consideration, allows us to obtain the annual (seasonal) percentage of rainfall associated with MCSs,  $P_{AM}$  ( $P_{SM}(i)$ ):

$$P_{AM} = \frac{\sum_{j=1}^{N_{AM}} p_j}{\sum_{l=1}^N p_l} \times 100, \quad (6)$$

$$P_{SM}(i) = \frac{\sum_{j=1}^{N_{SM}} p_j}{\sum_{l=1}^{N_S} p_l} \times 100, \quad (7)$$

where  $N_{AM}$  and  $N_{SM}$  represent the total number of days with MCSs for the year and for the season, respectively. In the same way, the hourly percentage of annual and seasonal precipitation related to MCS activity for each hour  $k$  considered is obtained,  $P_{AHM}(k)$  and  $P_{SHM}(ik)$ :

$$P_{AHM}(k) = \frac{\sum_{j=1}^{N_{AM}} p_{jk}}{\sum_{l=1}^N p_{lk}} \times 100, \quad (8)$$

$$P_{SHM}(ik) = \frac{\sum_{j=1}^{N_{SM}} p_{jk}}{\sum_{l=1}^{N_S} p_{lk}} \times 100. \quad (9)$$

### 3. Results and Discussion

In this section, in order to determine the impact of MCS activity on the diurnal variability of meteorological parameters and to assess the link between regional circulation and MCS activity and atmospheric instability, we divided our datasets into two samples: a sample associated to MCSs activity and a second, relative to the nonoccurrence of MCSs. Thus, for a description, in our work:

- (1) MCS activity (referred to as “MCSs” or “with MCSs” in the figures in this section) refers to the occurrence of at least one MCS within 24 hr over Yaounde. All analyses here are made for dates on which MCSs were recorded during the study period.
- (2) Non-MCS activity (referred to as “no MCS” or “without MCS” in the figures of this section) refers to the absence of MCSs within 24 hr over Yaounde. The corresponding analyses are made for dates where there is no MCS activity during our study period. Thus, non-MCS indicates other activities not identified



in this study that are not MCS activity or the possible absence of convective activity over Yaounde.

### 3.1. MCSs Activity and Impact on Environmental Conditions

**3.1.1. Diurnal Cycle of the Number of MCSs.** As shown by Jackson et al. [25], CA is a hotspot for MCS activity. Based on the analysis of Meteosat imagery, 623 MCS cells were recorded over Yaounde during the study period. The diurnal cycle of MCS occurrence in Yaounde (Figure 2(a)) shows minimal activity in the morning and substantial activity during the night. In fact, a total of 377 MCSs were recorded in the study area between 1,600 and 2,200 LT over the 2-year study period. Consequently, 60.51% of the 2-year cumulative sum of MCSs is observed during the late afternoon. In contrast, 55 (8.83% of the 2-year cumulative sum of MCSs) and 153 (24.56% of the 2-year cumulative sum of MCSs) were recorded in the morning (1,000–1,300 LT) and at night (0100–0400 LT), respectively, over Yaounde. This finding is in agreement with the results of previous studies [7, 25, 31, 39], except that these studies report maximum activity between 1,600 and 1,900 LT, while Figure 2(a) shows a maximum between 1,600 and 2,200 LT. This lengthening of the period of maximum MCS activity could be explained either by an increase in the number of MCSs, by an increase in their duration, or by both, according to Hu et al. [49]. Furthermore, the atmospheric conditions in a region are likely to influence both the duration and intensity of the MCSs that form there [23]. Therefore, a study of the environmental conditions and precipitation associated with MCSs should provide us with information about this fact.

**3.1.2. Environmental Conditions during the MCS and Non-MCS Occurrence.** This section analyses the atmospheric conditions associated with the sample of 623 MCSs, together with days with no MCS activity.

A novel component of this study is access to high-time resolution station data, which is sparse in CA. In this section, we exploit that the data to show associations in the diurnal cycle of relative humidity, dew point (Td), solar radiation, surface temperature, and wind speed on MCS days and no MCS days.

Figure 2 shows a significant variation of surface meteorological parameters during MCS activity over the city. Thus, MCSs are associated with an increase in the value of some meteorological parameters, while others show a decrease. In fact, higher values of relative humidity are observed on days with MCS at almost all hours, especially between midday and midnight (Figure 2(b)). The minimum humidity on days without MCS is about 5% lower than on days with MCS, and this can be seen in the afternoon, from 13:00 LT, and more clearly in the hours before the peak (1,200–1,500 LT). With the decrease in MCS activity during the night, the difference in relative humidity values between MCS and non-MCS days decreases progressively and is lower in the morning. The increase in surface humidity associated with MCSs is consistent with the findings of Feng et al. [23], who showed that the increase in MCS activity was associated with an increase in low-level humidity. Assuming that they also

found an increase in MCS precipitation in this environment, the observed increase in surface air humidity could have to deal with that.

In our sample, the higher values of Td for MCS days between 0700 and 2,000 LT (Figure 2(c)) are consistent with the observed increase in humidity, as the higher the dew point rises, the greater the amount of moisture in the air, and could follow the same explanation. Thus, the minimum and maximum of Td are around 19.78 and 21.10°C, respectively, for MCS days, while the corresponding values are lower at 19.69 and 20.78°C in the absence of MCS activity.

Furthermore, the solar radiation shows two clear characteristics (Figure 2(d)). Between 0500 and 1,000 LT, solar radiation is higher on MCS days, while between 1,100 and 1,700 LT, solar radiation is higher on non-MCS days. A plausible explanation for this is the formation of the convective cells that make up MCS in the early afternoon. The clouds increase the albedo and thus reduce the solar radiation received by the surface. The higher early morning solar radiation during the presence of MCS suggests that the development and/or arrival of MCS over the city is preceded by a relatively clearer sky, indicating low cloud cover compared to days without MCS. The presence of MCSs alters the diurnal cycle of solar radiation, resulting in higher solar radiation intensity during the first half of the cycle on days with MCSs, followed by the opposite trend in the second half. This pattern is also observed for surface temperature (Figure 2(e)), with higher afternoon temperatures on days without MCSs. The temperature in the presence of MCS remains significantly lower until about 1,900 LT when it gradually increases during the night to be slightly higher in the early morning than in the absence of MCS. The temperature difference with dates without MCSs, statistically significant at a 99% confidence level (not shown), can exceed 1.6°C and suggest considerable air cooling during MCS activity.

MCS activity also affects wind speed. Thus, there is an overall increase in the amplitude of the diurnal cycle of wind speed when MCS are recorded in Yaounde (Figure 2(f)) throughout the MCS sample inducing relatively higher wind speeds at the surface. These features could be explained by the strong vertical wind shear in the lower troposphere that has been previously identified during MCS activity [50]. Indeed, strong vertical wind shear at the surface, in addition to the presence of dry air in the mid-troposphere, favours the formation of MCSs [3].

Overall, the MCS activity induces a variation in surface meteorological parameters, and the direction of the variation varies from one parameter to another (Figure 3). However, the common variation of parameters during MCS activity reveals links between certain parameters that could explain the significant precipitation associated with MCSs. For example, the increase in the value of the dew point temperature coupled with the decrease in the value of the surface temperature observed during the MCS activity (Figures 2(c) and 2(e)) reflects a weak dew point depression. The latter, consistent with the lower tropospheric cooling associated with the observed increase in humidity, could further fuel moist deep convection [51] and could be associated with the lengthening

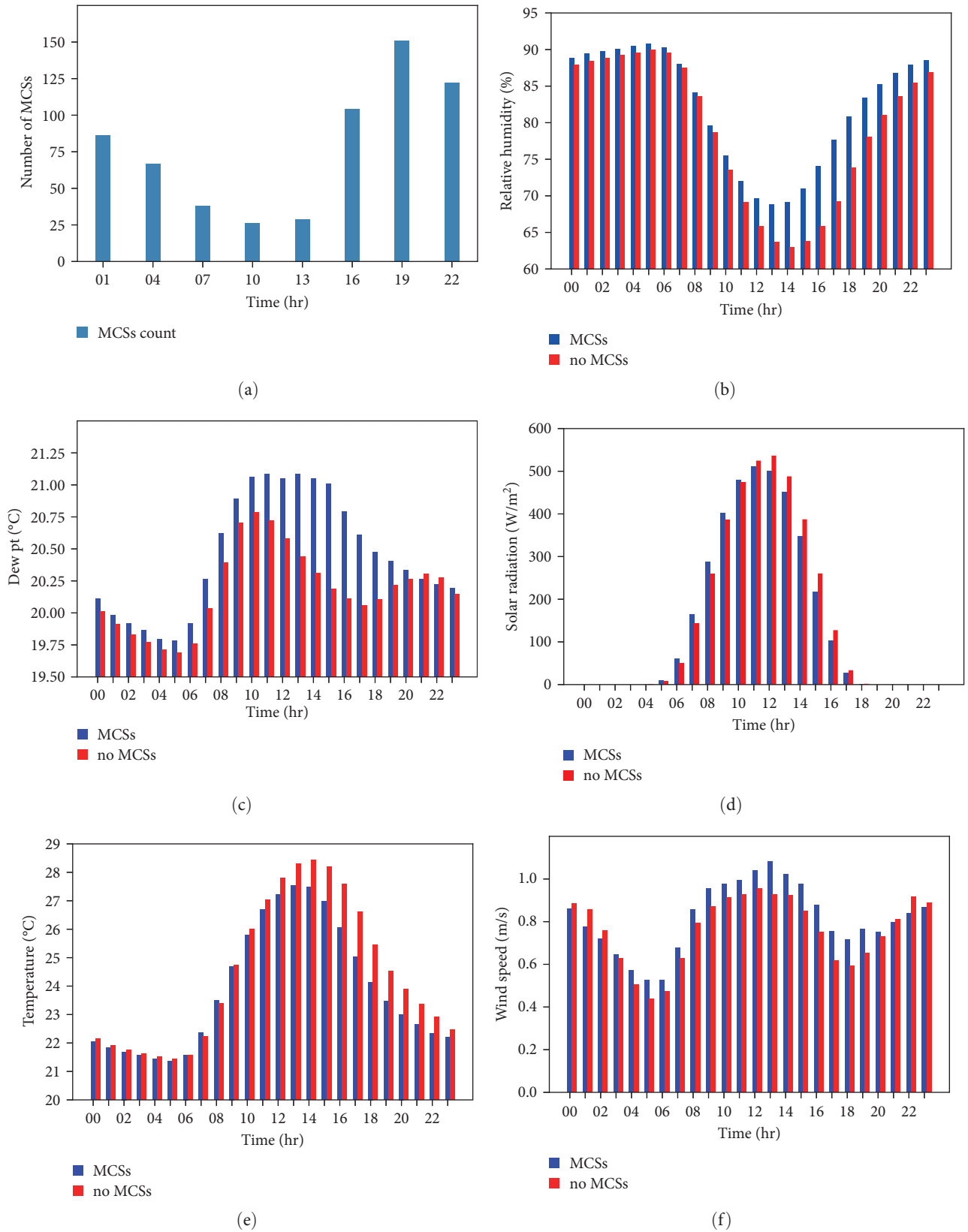


FIGURE 2: Diurnal cycle of (a) the relative number of MCSs in 3-hr intervals and the averages of (b) relative humidity, (c) dew point, (d) solar radiation, (e) surface temperature, and (f) wind speed in Yaounde for dates with and without MCSs during the study period.

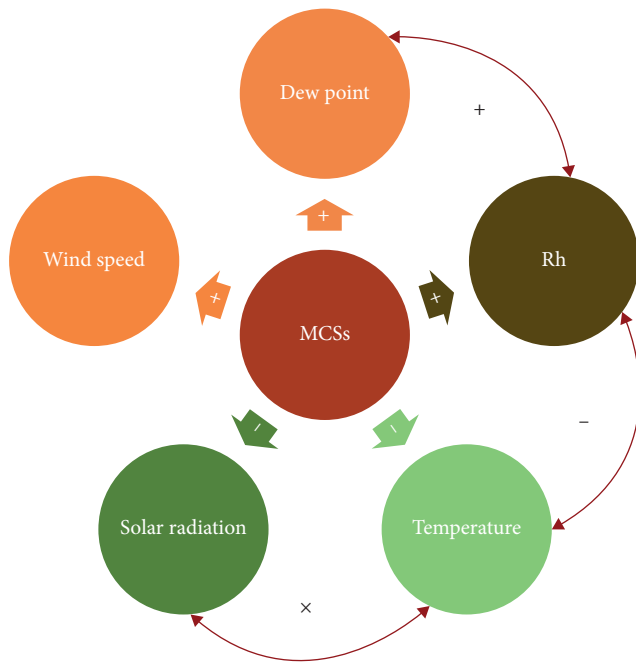


FIGURE 3: Influence of MCS's activity on the variation of surface meteorological parameters in Yaounde. The signs in the solid arrows indicate the effect of MCSs on the meteorological parameters. The linear arrows show the interactions between parameters.

of the period of maximum MCS activity as well as heavy associated rainfall.

### 3.2. Rainfall Associated with MCSs Activity in Yaounde

**3.2.1. Diurnal Cycle of Rainfall in Relation to the Activity of MCSs.** Averaged over 2 years, more than 57% of rainy days (Table 1) and more than 67% of total precipitation (Table 2) are related to MCSs, pointing to the importance of these systems in precipitation climatology. This result compares with the 60%–70% found in previous studies [11, 25, 31].

Figure 4(a) shows the diurnal cycle of rainfall in Yaounde for days with and without MCSs. A clear difference can be observed between the two cases: The intensity of rainfall is higher with the occurrence of MCSs, and especially during the night (between about 2,100 and 0500 LT throughout the sample). In addition, precipitation due to MCSs has two daily peaks (in the afternoon and at night), while precipitation without MCSs has only one peak (in the afternoon). This pattern of MCS rainfall could increase the total amount of rainfall with a direct consequence of increasing the risk of flooding, particularly in urban areas where impervious surfaces lead to rapid runoff and limited infiltration, according to Feng et al. [52].

It is interesting to note that while there were small differences in temperature and dew point temperature on MCS vs. no-MCS days, this converted into marked differences in rainfall intensity, which were statistically significant at a 99% confidence level (not shown). This may be due to the fact that dew point depression rather than absolute dew point is a good predictor of rainfall intensity [53, 54]. Assuming the effect of more moisture (an indicator of lower dew point depression) in the lower troposphere on the height of lifted

condensation levels, which is an important modulator of severe thunderstorms, lower dew point depression during MCS activity could be associated with heavier rainfall. However, even if MCS rainfall dominates for most of the cycle, non-MCS rainfall can also dominate, especially in the afternoon. This is the case, for example, at 1,400 LT when non-MCS rainfall exceeds MCS rainfall by more than 25 mm. This observation confirms the idea that other factors contribute significantly to rainfall in Yaounde.

The observed two daily rainfall peaks are consistent with the lengthening of the period of maximum of MCSs and may reflect an increase in the duration and frequency of precipitation due to MCSs, which could be due to an increase in the frequency and duration of individual storms [49]. Regarding the significant contribution of non-MCS rainfall to total afternoon rainfall, one possible explanation for this feature is the role of Yaounde's orography (Figure 1) in triggering isolated convection due to the thermodynamic response of the strong diurnal cycle of the Earth's surface temperature in a moisture-saturated environment [22, 39].

However, the average number of days with MCSs is higher than the number of rainy days due to MCSs (Table 3). It is plausible that:

- MCS activity is not always synonymous with precipitation.
- There may be a time lag between MCS's activity and the precipitation they generate.

The former is reinforced by the results of Kuete et al. [55], who showed that convection in CA could be either dry or wet depending on whether the jet intensity is strong or weak. This could explain why on several dates, MCS's activity did not lead to rainfall. Furthermore, given the lower dew point depression during MCS activity and the high saturation of the atmosphere, large-scale disturbances may not be necessary for precipitation formation. Alternatively, the development of MCS may be suppressed. The atmospheric conditions, which vary during MCS activity (Figure 3), could promote or inhibit the contribution of MCSs to local precipitation.

**3.2.2. Frequency of Occurrence of MCSs and Percentage of Associated Precipitation.** Figure 4(b) shows the diurnal cycle of MCS occurrence frequency coupled with rainfall associated with MCS activity in Yaounde. In our sample, fairly high percentages of precipitation are observed during the night between 0100 and 0700 LT, with values above 80%. However, this maximum is not consistent with the frequency of occurrence of MCS, which like MCS activity, has its maximum earlier in the afternoon. The daily maximum of precipitation associated with MCSs does not coincide with the peak of their activity. This is in line with the hypothesis posed above regarding the possible time lag that would exist between the peak of MCS activity and the precipitation associated with it. This time lag could also explain the rather considerable percentage values recorded between 1,000 and 1,300 LT, when the frequencies of occurrence are at their lowest, and is in agreement with the results of Nesbitt and Zipser [31] and

TABLE 1: Percentage of rainy days and rainy days with MCSs in Yaounde.

Year	Period	Number of days	Number of MCSs	Number of rainy days	Percentage of rainy days	Percentage of rainy days with MCSs	Gap percentage
2019	Annual	365	307	172	47.64	61.04	1.22
	First wet season	103	132	62	60.19	74.19	2.59
	Second wet season	86	93	55	63.95	63.63	0
2020	Annual	366	316	130	35.51	52.30	6.04
	First wet season	68	102	37	54.41	78.37	1.41
	Second wet season	52	67	26	50	61.53	31.28

TABLE 2: Annual and seasonal averages of MCSs occurrence frequencies and associated rainfall percentages.

Year	Period	MCSs occurrence's frequency (%)	Total rain due to MCSs (mm)	Total rain (mm)	Percentage of rain due to MCSs
2019	Annual	10.48	1,102	1665.8	66.15
	First wet season	15.86	551.2	613.8	89.80
	Second wet season	13.36	410.6	628.6	65.31
2020	Annual	10.76	826.6	1,203	68.71
	First wet season	18.22	378.6	404	93.71
	Second wet season	15.80	224.4	277	81.01

those of Maranan et al. [24], who observed a 2-hr lag between the passage of the MCS core and the detection of rainfall.

**3.3. MCS, Precipitation, and Seasonality.** CA experiences two distinct rainy seasons, each with its own characteristics and impacts on rainfall [56]. In this section, we define the rainy seasons for 2019 and 2020 based on AWS data before analysing the seasonal characteristics of MCS events and their contribution to local rainfall.

**3.3.1. Onset and Cessation of Rainy Seasons.** To establish the rainfall climatology in Yaounde during the study period, Figure 5 shows the cumulative average daily rainfall anomaly, which allows the definition of the onset and cessation dates of the rainy seasons in 2019 and 2020. For both years, there are two anomaly peaks corresponding to the retreat of the rainy seasons characteristic of the bimodal regime in Yaounde, with one short and one long rainy season per year [29, 30]. The year 2020 has much shorter (longer) rainy (dry) seasons than 2019.

In addition to being longer, the rainy seasons are earlier in 2019 compared to 2020. There is a difference of almost a month between the start of the rainy seasons (short and long) for the 2 years. In 2019, the short rainy season starts on 8 March compared to 9 April for 2020. The major rainy season starts on 19 August and 14 September in 2019 and 2020, respectively. However, 2019 and 2020 have annual rainfall variability close to the Central African climatology described in previous studies [7, 25, 39, 56].

**3.3.2. Seasonality of MCSs Activities and Rainfall.** To examine the seasonality of MCS in Yaounde, Figure 6 shows the diurnal cycle of seasonal MCS number, frequency of

occurrence, percentage of associated rainfall, and total rainfall due and not due to MCS. As observed for the whole sample (Figure 2(a)), for both wet seasons, MCS activity peaks between 1,600 and 2,200 LT, is minimal in the morning and substantial at night (Figure 6(a)). The total number of MCSs recorded in the late afternoon during the first and second rainy seasons, respectively, were 125 and 123, representing 53.41% and 70.63% of the 2-year cumulative sum of MCSs observed during the respective season over the 2-year study period. Conversely, during the morning, 17 and 6 MCSs were observed, respectively, representing 7.26% and 3.75% of the seasonal cumulative sum. During the night, relatively moderate values are recorded, with 72 in the first season and 35 in the second. These values represent 30.77% and 21.87% of the 2-year seasonal cumulative sum of MCS events, respectively. However, during the first rainy season, MCS activity is more frequent through the night compared with the second season, where the decline in activity through the night is marked. And this is consistent with the higher values of the frequencies of occurrence recorded during the first season compared to the second rainy season (Table 2). The difference in MCS occurrence between the two rainy seasons is greatest between 0100 and 1,000 LT, when the differences can exceed 50% (Figures 6 (d) and 6(e)).

Figure 6 also shows that from the two daily peaks in MCS rainfall, the nocturnal one appears to derive mainly from the first rainy season (Figure 6(b)) compared to the second (Figure 6(c)). In addition, the first wet season records the highest percentage of rainy days with MCSs (Table 1) for both years, as well as the greatest number of MCSs (Tables 1 and 3). This matches the higher percentage of precipitation due to MCSs observed during this season compared to the second season (Figures 6(d), 6(e), and Table 2). Thus, the



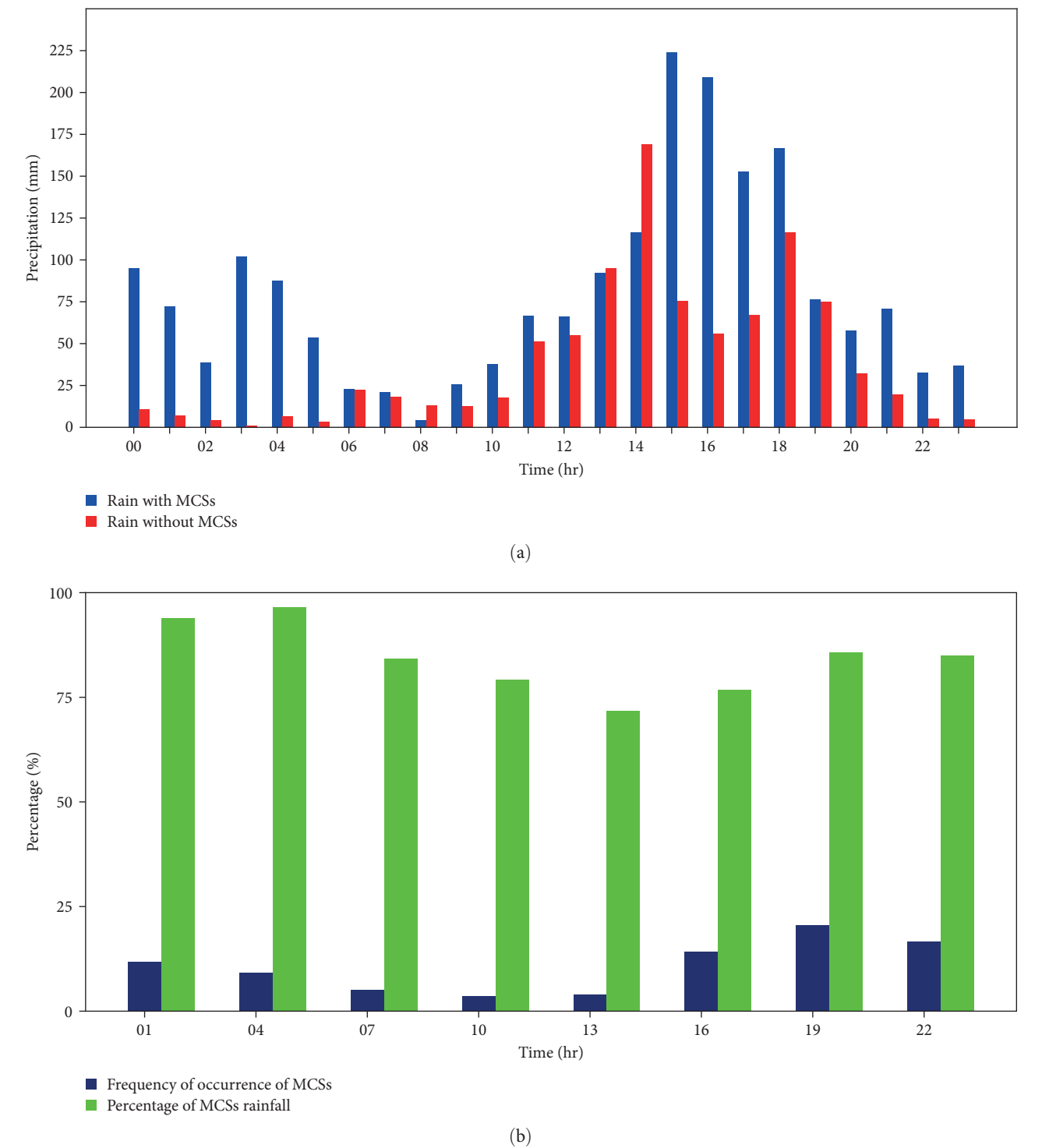


FIGURE 4: Diurnal cycle of (a) total rainfall in Yaounde for dates with and without MCSs and (b) the hourly averages of MCS occurrence frequency and percentage of associated rainfall over the study period.

increase in the frequency and duration of individual storms explaining the increase in the frequency and duration of precipitation due to MCSs, according to Hu et al. [49], and a possible factor in the two daily peaks, should be more marked during the first rainy season.

The ability of MCSs to generate heavy rainfall, both on an annual (more than 60%) and seasonal (more than 80%,

consistent with Andrews et al. [8]) scale, due to the high percentage of associated rainfall, suggests that MCSs could increase the risk of flooding events over the city of Yaounde. This rain-inducing effect of MCSs may be more pronounced during the first rainy season. The large amount of water produced by MCSs is beneficial for agricultural development, as Cameroon's economy is heavily dependent on rain-fed

TABLE 3: Seasonal variations of MCSs and rainfall associated with MCSs between 1,600 LT and 2,200 LT in Yaounde.

Year	Period	Number of days with MCSs	Total number of MCSs	Number of raining days with MCSs	Total rain due to MCSs
2019	First wet season	41	67	23	233.8
	Second wet season	46	64	26	195.8
2020	First wet season	35	60	19	207.8
	Second wet season	30	49	10	124.8

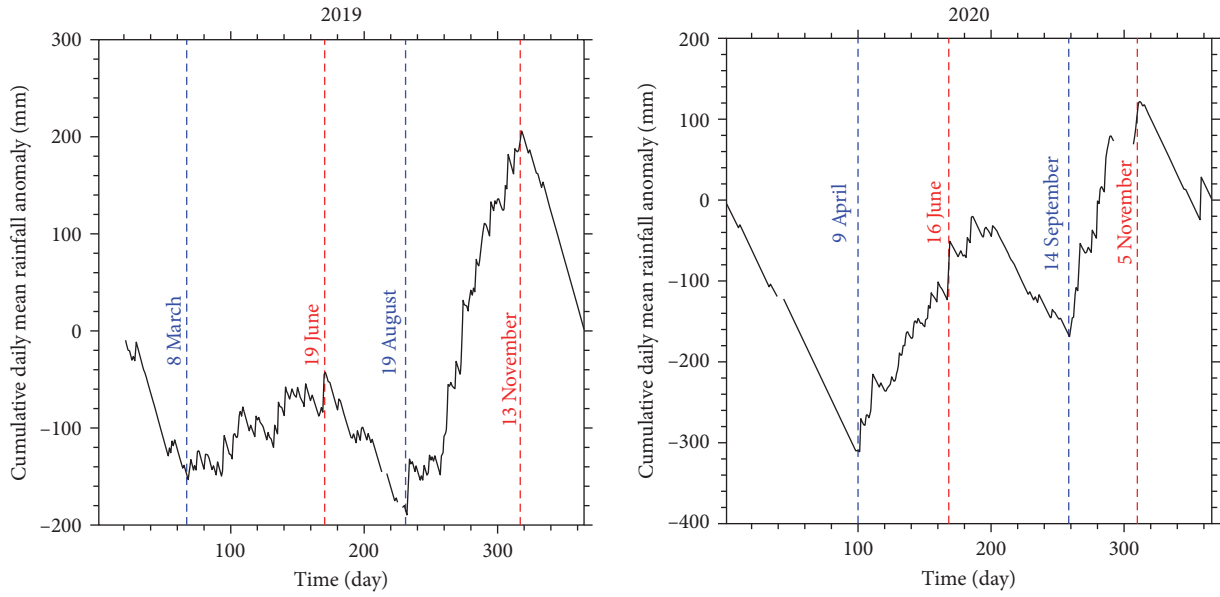


FIGURE 5: Yaounde cumulative mean daily rainfall anomaly, start (blue) and end (red) dates of rainy seasons for 2019 and 2020.

agriculture [57]. However, this water also leads to the risk of flooding, resulting in significant socioeconomic damages [27, 28]. The rapid and unplanned growth of the city as in many major cities of Africa, and the great capacity of MCS to trigger intense rainfall, further strengthens the motivation to investigate the link between MCS activities and the occurrence of extreme weather events in CA.

During the second rainy season (mainly in the afternoon), the majority of precipitation seems to be initiated by systems other than MCSs (Figure 6(c)). They sometimes produce more than 50 mm compared to MCSs. This observation, in addition to confirming the idea that other factors in Yaounde contribute considerably to rainfall, suggests that they are particularly active during the second wet season and in the afternoon. In addition, this season has a higher percentage of rainy days and total rain than the first wet season in 2019 (Tables 1 and 2). The opposite fact observed in 2020 is probably the result of the gaps observed in this season (Table 1). Possible factors explaining rainfall characteristics in the second season include orographic convection in a moisture-saturated environment [22, 39] due to the orography of Yaounde (Figure 1). As well as the maximum convergence of the mid-tropospheric moisture flux during the SON season [25, 56, 58, 59].

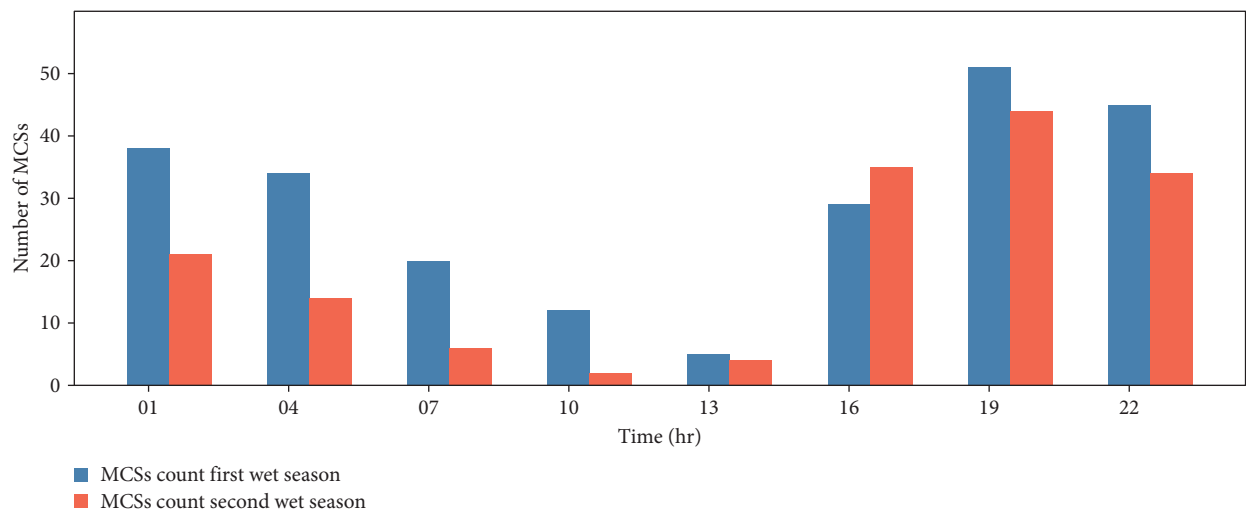
Furthermore, the seasonal averages of atmospheric parameters recorded at Yaounde between 1,600 and 2,200 LT for the

two seasons in 2019 and 2020 (Table 4) show higher seasonal averages for relative humidity during the second rainy season in both years. The air humidity is therefore higher in the second rainy season than in the first. The average dew point temperature is higher in the first season than in the second in both 2019 and 2020. The same applies to the average surface temperature and solar radiation. Thus, compared to the first rainy season, the second rainy season presents an atmosphere relatively closer to saturation: high relative humidity, high cloud cover, and a small difference between temperature and dew point. Thus, the atmosphere should be less unstable during the second rainy season due to the lower dew point depression and lower surface wind speed [50]. In addition, given the high saturation of the atmosphere, large-scale disturbances may not be necessary for precipitation to form, which explains the large amount of non-MCS rainfall during this season.

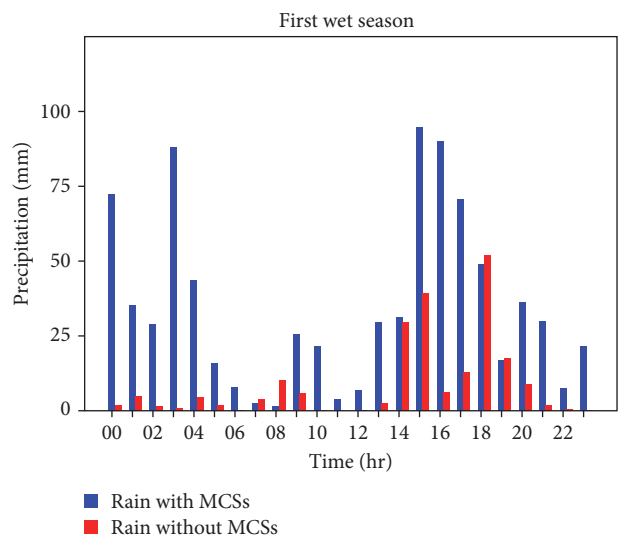
#### 3.4. MCSs's Activity, Atmospheric Stability, and Regional Circulation

**3.4.1. Equivalent Potential Temperature and MCSs's Activity.** The study of the atmospheric dynamics associated with MCS activity requires a separate analysis of the two rainy seasons, as they are associated with different climatic features.

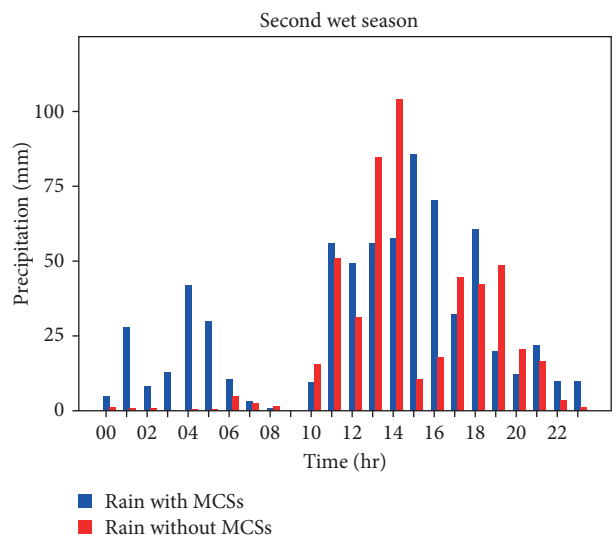
To examine the atmospheric stability during the activity of MCSs, Figure 7 shows the longitude–altitude cross section



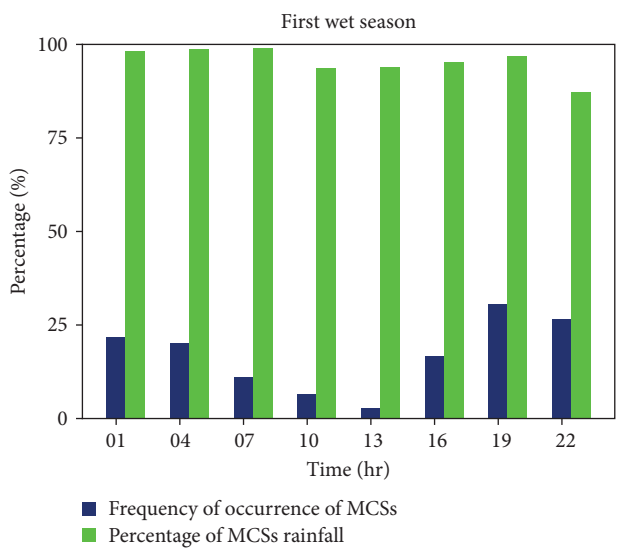
(a)



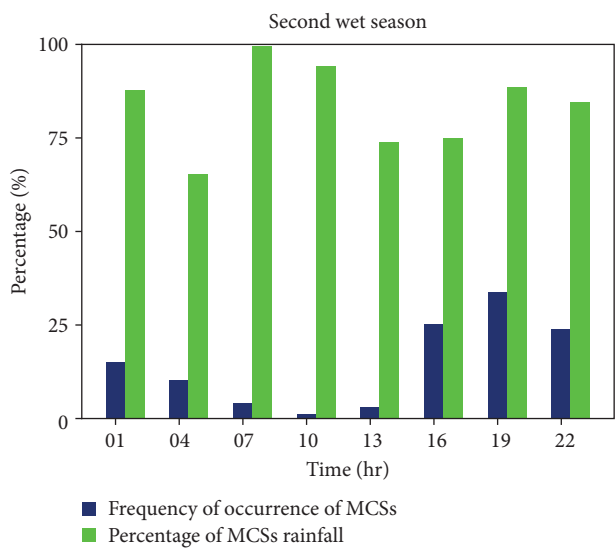
(b)



(c)



(d)



(e)

FIGURE 6: The diurnal cycle of seasonal (a) relative number of MCSs in 3-hr intervals, (b and c) total rainfall in Yaounde for dates with and without MCSs, and (d and e) hourly averages of MCS occurrence frequency and percentage of associated rainfall over the study period.

TABLE 4: Seasonal averages of atmospheric parameters associated with MCS activity in Yaounde between 1,600 and 2,200 LT.

Year	Period	Average relative humidity (%)	Average dew point temperature (°C)	Average temperature (°C)	Average dew point depression (°C)	Average solar radiation ( $\text{W}\cdot\text{m}^{-2}$ )	Average wind speed ( $\text{m}\cdot\text{s}^{-1}$ )
2019	First wet season	81.75	21.26	24.76	3.5	50.77	0.78
	Second wet season	83.76	20.14	23.12	2.98	30.50	0.75
2020	First wet season	79.12	20.96	24.97	4.01	72.73	0.75
	Second wet season	86.96	20.28	22.64	2.36	22.48	0.58

of the seasonal mean  $\theta_e$  in shade and the difference in  $\theta_e$  between days with and without MCSs in contour for the time slices with maximum (1,600–1,900 LT), minimum (1,000–1,200 LT), and substantial (0100–0300 LT) MCSs activity during the MAM and SON seasons in 2019 and 2020.

Equivalent potential surface temperature seen as an integrated measure of temperature and moisture changes [60], a guiding parameter of atmospheric convective instability and convective cloud penetration depth [60, 61, 62], represents a good measure of deep convection. When boundary-layer  $\theta_e$  increases, the CAPE follows the same evolution, also increasing the maximum altitude of the convective cloud top [63, 64].

In the lower troposphere, we observe a decrease in the seasonal average of  $\theta_e$  with altitude, synonymous with an unstable atmosphere. From  $\partial \theta_e / \partial z < 0$ , there is convective instability in the lower troposphere during both rainy seasons. And as shown by Hartman [7], this instability is more pronounced in MAM than in SON, but this seems to contradict the results of previous studies [11, 25, 31, 39], which have shown an intensification of convective activity during the SON season.

However, both the MAM and SON seasons show an increase during the day in  $\theta_e$  in the lower troposphere, with the highest values in the 1,600–1,900 LT time slot. This period of maximum surface  $\theta_e$  coincides with the period of maximum MCS activity [7, 25, 31, 39]. As MCSs are indicators of deep convection, we observe an overall increase in  $\theta_e$  during MCS activity (Figure 7). The decrease in  $\theta_e$ , compared to days without MCSs, in the lower troposphere is consistent with the lower temperature (Figure 2(e)) and higher humidity (Figure 2(b)) at the surface observed during MCS activity. These two factors combined lead to a higher density of the surface air during MCS activity.

The decrease of  $\theta_e$  at the surface is accentuated in MAM and during the 1,600–1,900 LT time slot, a sign of stronger activity of the MCSs. Similarly,  $\theta_e$  shows, especially over land regions, a strong correlation with precipitation and CAPE [24, 60]; the increase in  $\theta_e$  during MCSs activity is associated with an increase in precipitation compared to days without MCSs as well as with higher precipitation due to MCSs in MAM than in SON (Figure 6).

Nevertheless, the lower instability and thus shallower convection during the SON season coincide with higher

seasonal totals (Table 2) and non-MCS (Figure 6) precipitation than during the MAM season. A possible explanation (in addition to the convergence of the moisture flux) for this observation can be found in the work of Fritz et al. [65], who found that of the three types of convection (shallow convection, mid-level convection, and deep convection), mid-level convection is the most frequent and contributes the most to total precipitation, although deep convection has the highest precipitation surface coverage rate. Furthermore, it has been observed that deep convection is not always a necessary condition for extreme precipitation [66]; thus, rain clouds with weak to moderate convective intensity are capable of producing intense precipitation [67, 68]. The enhancement of orography-driven precipitation is strongly involved in this process [69, 70]. Thus, rain clouds of a small spatial extent may have made a significant contribution to the total rainfall recorded during the SON season.

Overall, the favourable atmospheric conditions during MCS activity in both rainy seasons, such as high cloudiness (low solar radiation and low dew point depression, very high humidity (Table 4)) and high convergence of moisture flux, especially in SON [25, 56, 58, 59], combined with instability in the lower troposphere, can be associated with the presence of long-lasting MCS [23], which explains the longer period of maximum MCS activity (Figure 3). And could also explain the second daily peak in precipitation due to MCS (Figure 6), according to Hu et al. [49], who found a link between the increase in frequency and duration of MCS and those in associated rainfall.

**3.4.2. AEJ, MCSs Activity, and Link to Precipitation.** According to Nicholson and Grist [58], the CA rain belt lies between the cores of two mid-level jets: the AEJ-S and the AEJ-N. These two jets are best developed around 650 and 700 mb and migrate seasonally with the rain belt. Jackson et al. [25], by observing the AEJ-S during the wettest season in the CA (SON), concluded that the latter could play a role in the anomalous intensity of convection in this region. In this section, we will verify the link between MCSs and the AEJ.

Figure 8 shows the annual evolution of wind intensity at 600 hPa for the years 2019 and 2020. The presence of the AEJ-S can only be observed during one season of the year, from September to November. The absence of this jet during



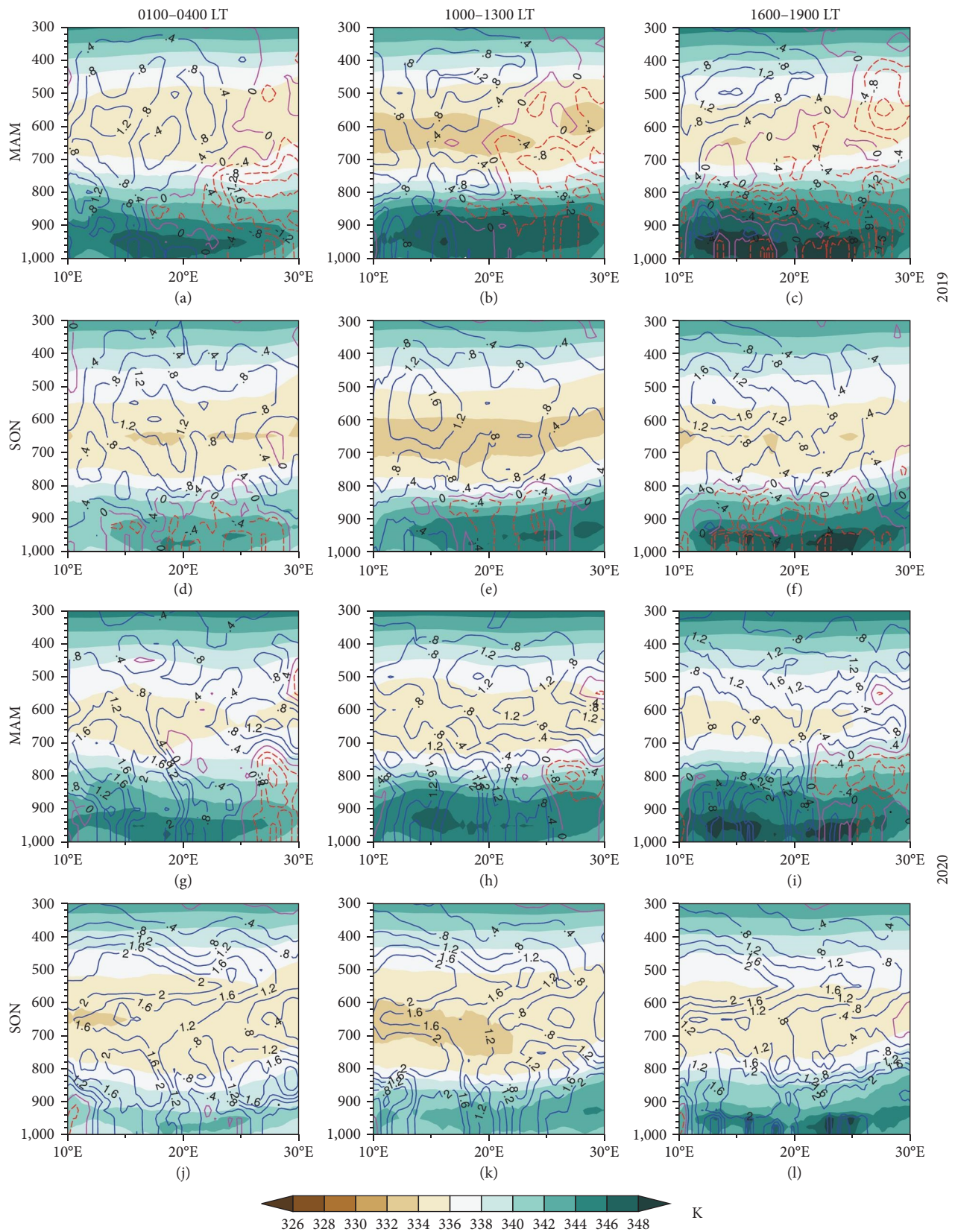


FIGURE 7: Longitude–altitude cross-section of the seasonal average  $\theta_e$  (in K, shaded) and the difference in  $\theta_e$  between days with and without MCSs (contours) averaged between 3.25–5°N; for the maximum (1,600–1,900 LT, (c, f, i, and l)), minimum (1,000–1,300 LT, (b, e, h, and k)), and substantial MCS activity (0100–0400 LT, (a, d, g, and j)) from the ERA5 reanalysis dataset.

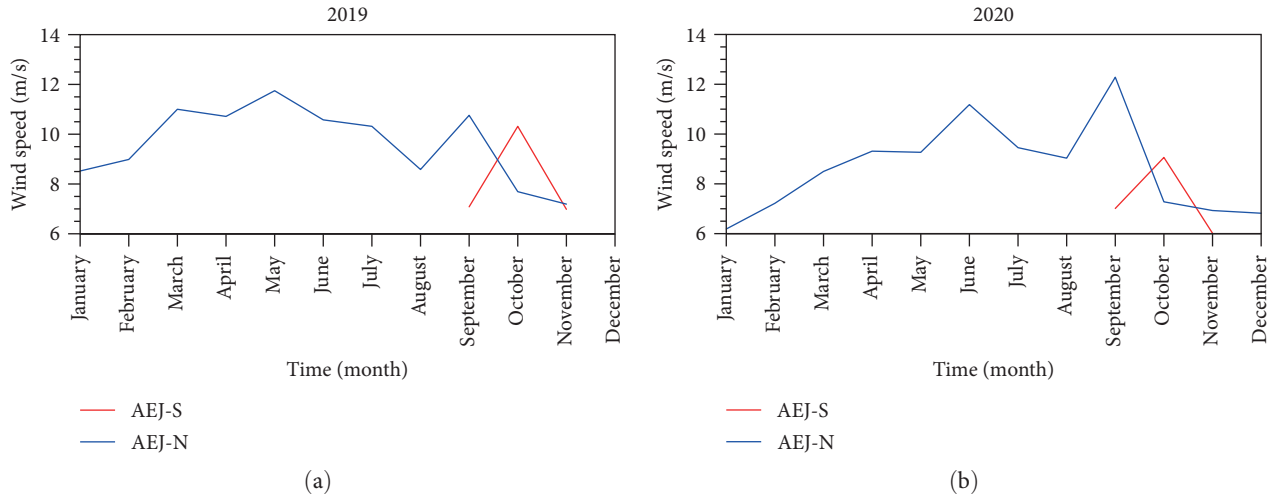


FIGURE 8: Evolution of the intensity over the year of the two components of the AEJ at 600 hPa in 2019 (a) and 2020 (b) from the ERA5 reanalysis dataset.

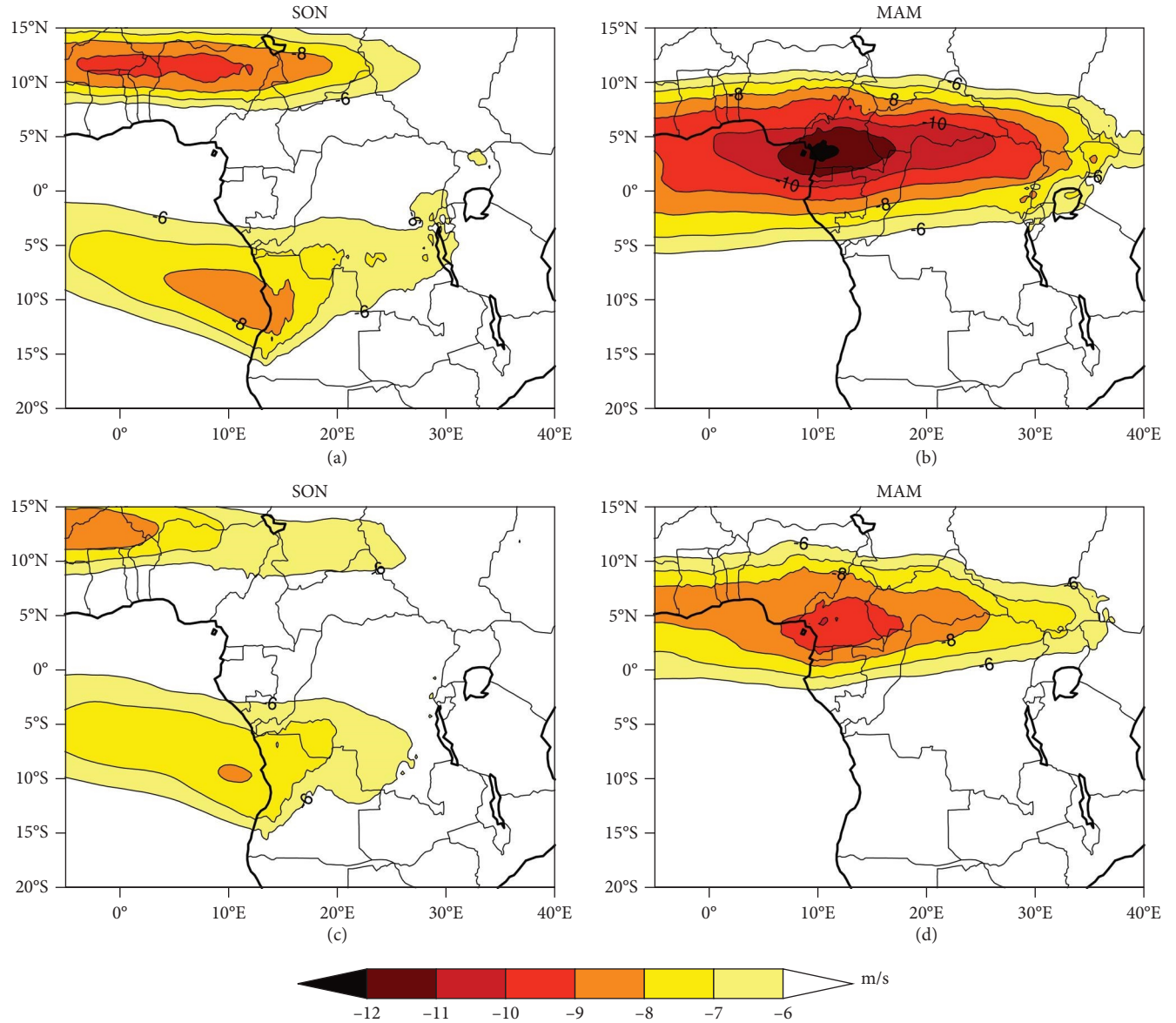


FIGURE 9: Spatial distribution of zonal wind intensity (m/s) at 600 hPa in 2019 (a and b) and 2020 (c and d) for the SON (a and c) and MAM (b and d) seasons from the ERA5 reanalysis dataset.

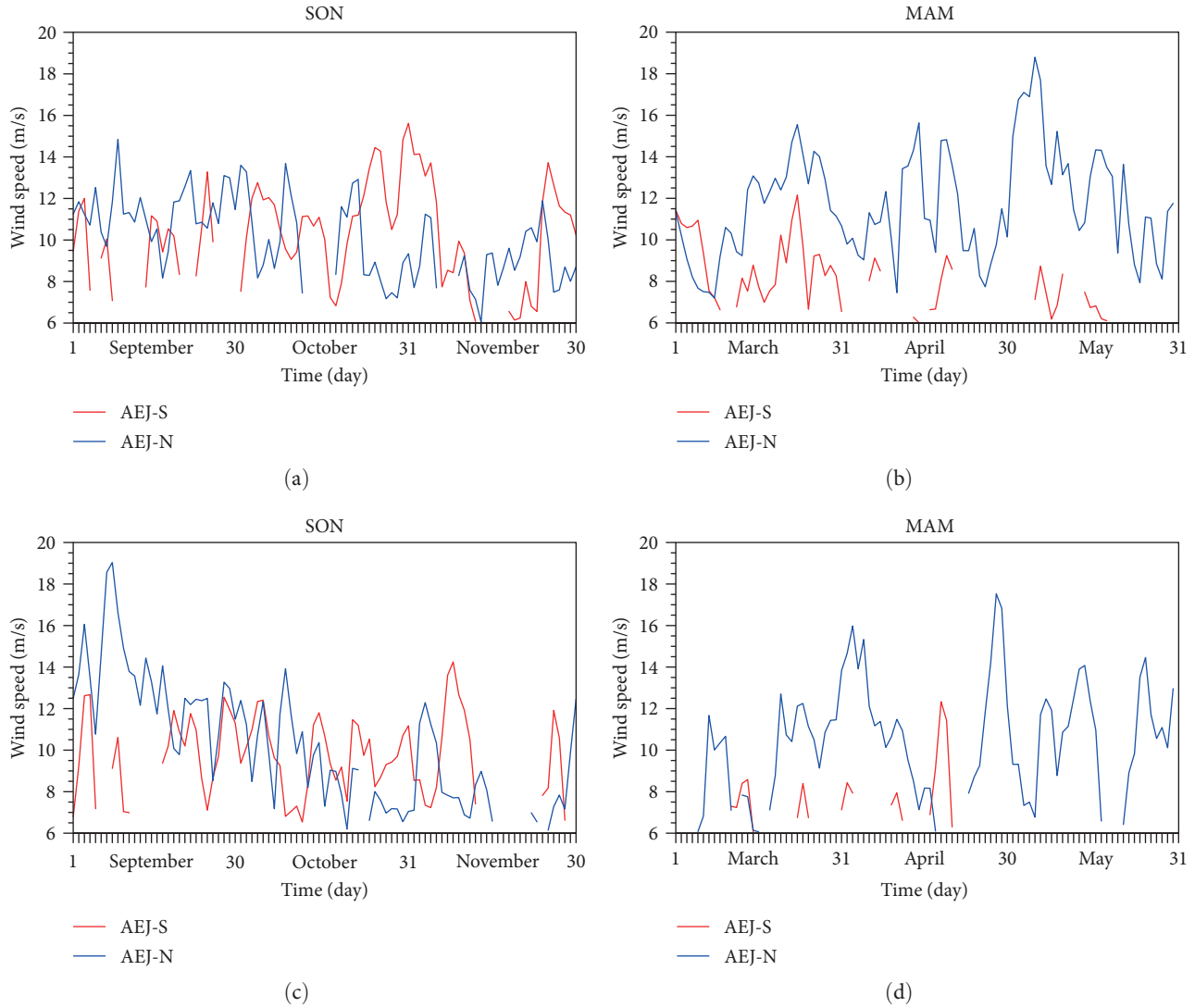


FIGURE 10: Evolution of the intensity during the SON and MAM seasons of the two components of the AEJ at 600 hPa in 2019 (a and b) and 2020 (c and d) for the SON (a and c) and MAM (b and d) seasons.

the rest of the year is in agreement with the results of studies on this component of the AEJ [25, 55, 58], which showed that a mid-tropospheric easterly jet, analogous to the African easterly jet in the Northern hemisphere, is clearly defined during the September to November season. The northern component is present throughout the year.

The presence of both jets during the SON season enhances convection during this season in the band between the cores of the two jets located on average at  $10^{\circ}\text{N}$  and  $10^{\circ}\text{S}$  for the Northern and Southern jets, respectively (Figure 9). Indeed, the conceptual four-quadrant model developed by Uccellini and Johnson [71] prescribes for a southern hemisphere jet a convergence in the right entrance region, a divergence in the left entrance region, and the opposite pattern in the northern hemisphere. Thus, we should get more precipitation in SON because our study area is in the rain belt between the AEJ-S and AEJ-N cores [25, 26], and this is the case in 2019 (Table 2). Nevertheless, it is also interesting to note that the presence of the two AEJ components in the same year coincides with the

highest values of non-MCS precipitation in the afternoon (Figure 6). Moreover, in the MAM season, the AEJ-N is quite strong on most days, with values above 8 m/s (Figure 10), which is consistent with its position over the city (Figure 9). And could be related to the stronger convective instability in this season (Figure 7) and the highest rainfall due to MCS (Figure 6 and Tables 3 and 2). In addition to providing moisture, the AEJ also provides lift and wind shear to the atmosphere, all of which are essential ingredients for convection and rainfall [55].

This is not consistent with the results of Jackson et al. [25], who showed that the fourth maximum of MCS activity in West Central Africa coincides with a mid-tropospheric convergence maximum in the right entrance quadrant of AEJ-S. Thus, the strong convergence of the moisture flux could drive local atmospheric conditions in the SON, which could limit not only the activity of the MCSs but also their contributions to precipitation.

However, the presence of one or both components of the AEJ on almost all days during both rainy seasons (Figure 10)



is not only consistent with the occurrence of more than 60 MCSs recorded in these seasons (Table 1) but also with the large contribution of MCSs to total rainfall (Table 2). This finding is consistent with the ability of AEJ-N and AEJ-S to positively influence the intensity and evolution of MCSs and their ability to produce heavy rainfall [22, 25, 72].

#### 4. Conclusion

This study focused on the analysis of MCS activity over the city of Yaounde. It was done using data from the automatic weather station of the higher teacher training college of the University of Yaounde 1, data from the online MCS count on the EUMeTrain website, and ERA5 reanalysis data from the European Copernicus website. We conducted our study over a 2-year period: 2019 and 2020. Our goals were to determine the frequency of occurrence of MCSs, the percentage of local precipitation due to MCSs, their impact on the evolution of surface meteorological parameters, their relationship with large-scale circulation, and the stability state of the atmosphere linked to their activity.

The results show that MCS activity is highest in the afternoon (1,600–2,200 LT), lowest in the morning (1,000–1,300 LT), and substantial at night (0100–0400 LT; Figure 2). The extension of the period of maximum MCS activity to 2,200 LT is one of the changes from previous studies [7, 25, 31, 39]. It could be due to the ability of favourable atmospheric conditions (lower dew point depression and higher relative humidity) combined with the orography of Yaounde to induce long-lasting and/or more intense MCS [23]. Indeed, MCS activity over Yaounde is associated with an increase in the values of some parameters (relative humidity, dew point temperature, and wind speed), while others show a decrease in their values (solar radiation and surface temperature; Figure 2). There is a relationship between the variations of some parameters, which has made it possible to establish that the decrease and the respective increase in temperature and dew point in the lower troposphere (low dew point depression) associated with an increase in the humidity of the air observed during MCS's activity could be at the origin of the heavy rainfall associated with them. Similarly, the lengthening of the period of maximum MCS activity could be related to the existence of two daily peaks of precipitation due to MCSs (the first peak in the afternoon and the second at night) compared to a single peak for those not due to MCSs (only one peak in the afternoon). This would reflect the effect of the duration and frequency of MCSs on that of associated precipitation [49]. The time lag between the peak of MCS activity and that of associated rainfall found could also have to deal with that.

A comparison between precipitation due to and not due to MCSs shows that MCSs contribute strongly to the precipitation recorded in Yaounde, producing more than 60% of the total annual precipitation and more than 80% during the rainy seasons (Table 2). This high contribution, which is consistent with the high activity of the MCS over the city (more than 60 MCS occurrences for each season (Table 1)), is associated not only with strong convective instability in the lower troposphere but also with the presence of one or both

components of the AEJ. Moreover, the double vs single rainfall pattern with and without MCSs exhibits a difference in MCS rainfall-triggered capability between the two rainy seasons. The first rainy season shows a dominance of double-peak MCSs rainfall pattern while the second shows a dominance of single-peak non-MCSs rainfall pattern.

The state of stability in the lower troposphere is strongly conditioned by the diurnal cycle of MCS activity, with the strongest convective instability during the afternoon peak of MCS activity. The strongest instability during the MAM season (first rainy season) matches the location of the AEJ-N core over Yaounde, as well as the more intense MCS activity and the heaviest associated precipitation with a double-peak rainfall pattern dominance. It should also be noted that the presence of both components of the AEJ in SON is found to be accompanied by an increase in single-peak non-MCS precipitation during the second rainy season. This suggests not only that atmospheric conditions may favour or inhibit the contribution of MCS to local precipitation, but also that there are factors other than MCS that contribute significantly to precipitation during this season. The topography of Yaounde and the presence of the two components AEJ may be the determining factors in the formation of this type of convective cell.

This study demonstrates the ability of MCSs to influence rainfall patterns in CA and shows the importance of considering the environmental meteorological parameter condition when assessing the rain-induction capacity of MCSs in a given location. In the context of a changing climate with rapid land-use changes, it is critical to improve our understanding of this interaction.

#### Data Availability

The MCS data were collected using the EUMeTrain MapViewer module (<http://www.eumetrain.org/ePortMapView/r/index.html>). The ERA5 reanalysis is provided by the Copernicus Change Service (C3S) of ECMWF and is available at <https://cds.climate.copernicus.eu/cdsapp#!/dataset/>.

#### Disclosure

This work was submitted as an abstract to participate in the 3rd Workshop on Cloud Organization and Precipitation Extremes—WCO3 which took place on 4–8 September 2023, in Trieste, Italy, at the International Centre for Theoretical Physics (ICTP) as per the link (<https://indico.ictp.it/event/10204/material/8/0.pdf>).

#### Conflicts of Interest

The authors declare that they have no conflicts of interest.

#### Acknowledgments

The authors would like to thank Eumetrain for the availability of online satellite data via the Eumetrain MapViewer module.



## References

- [1] R. A. Houze Jr., "Mesoscale convective systems," *Reviews of Geophysics*, vol. 42, no. 4, pp. 1–43, 2004.
- [2] W. Liu, K. H. Cook, and E. K. Vizy, "The role of mesoscale convective systems in the diurnal cycle of rainfall and its seasonality over sub-Saharan Northern Africa," *Climate Dynamics*, vol. 52, no. 1–2, pp. 729–745, 2019.
- [3] V. Mathon, *Etude climatologique des systemes convectifs de meso-echelle en Afrique de l'Ouest*, Ph.D. thesis Université Paris, 2001.
- [4] M. D. Parker, "Response of simulated squall lines to low-level cooling," *Journal of the Atmospheric Sciences*, vol. 65, no. 4, pp. 1323–1341, 2008.
- [5] H. Laurent, N. D'Amato, and T. Lebel, "How important is the contribution of the mesoscale convective complexes to the Sahelian rainfall?" *Physics and Chemistry of The Earth*, vol. 23, pp. 629–633, 1998.
- [6] V. Mathon and H. Laurent, "Life cycle of Sahelian mesoscale convective cloud systems," *Quarterly Journal of the Royal Meteorological Society*, vol. 127, no. 572, pp. 377–406, 2001.
- [7] A. T. Hartman, "Tracking mesoscale convective systems in central equatorial Africa," *International Journal of Climatology*, vol. 41, no. 1, pp. 469–482, 2021.
- [8] P. C. Andrews, K. H. Cook, and E. K. Vizy, "Mesoscale convective systems in the Congo Basin: seasonality, regionality, and diurnal cycles," *Climate Dynamics*, vol. 62, pp. 609–630, 2024.
- [9] R. C. Blamey and C. J. C. Reason, "Numerical simulation of a mesoscale convective system over the east coast of South Africa," *Tellus A: Dynamic Meteorology and Oceanography*, vol. 61, no. 1, pp. 17–34, 2009.
- [10] R. C. Blamey and C. J. C. Reason, "Mesoscale convective complexes over southern Africa," *Journal of Climate*, vol. 25, no. 2, pp. 753–766, 2012.
- [11] S. W. Nesbitt, R. Cifelli, and S. A. Rutledge, "Storm morphology and rainfall characteristics of TRMM precipitation features," *Monthly Weather Review*, vol. 134, pp. 2702–2721, 2006.
- [12] R. Roca, J. Aublanc, P. Chambon, T. Fiolleau, and N. Viltard, "Robust observational quantification of the contribution of mesoscale convective systems to rainfall in the tropics," *Journal of Climate*, vol. 27, no. 13, pp. 4952–4958, 2014.
- [13] Y. Chan, X. Chen, and L. R. Leung, "A high-resolution tropical mesoscale convective system reanalysis (TMeCSR)," *Journal of Advances in Modeling Earth Systems*, vol. 14, no. 9, Article ID e2021MS002948, 2022.
- [14] P. Bechtold, N. Semane, P. Lopez, J. P. Chaboureaud, A. Beljaars, and N. Bormann, "Representing equilibrium and nonequilibrium convection in large-scale models," *Journal of the Atmospheric Sciences*, vol. 71, no. 2, pp. 734–753, 2014.
- [15] R. Washington, R. James, H. Pearce, W. M. Pokam, and W. Moufouma-Okia, "Congo Basin rainfall climatology: can we believe the climate models?" *Philosophical Transactions of the Royal Society B: Biological Sciences*, vol. 368, no. 1625, Article ID 20120296, 2013.
- [16] C. M. Taylor, D. Belušić, F. Guichard et al., "Frequency of extreme Sahelian storms tripled since 1982 in satellite observations," *Nature*, vol. 544, no. 7651, pp. 475–478, 2017.
- [17] G. Xu, T. Dong, P. B. Cobbinah et al., "Urban expansion and form changes across African cities with a global outlook: spatiotemporal analysis of urban land densities," *Journal of Cleaner Production*, vol. 224, pp. 802–810, 2019.
- [18] G. Di Baldassarre, A. Montanari, H. Lins, D. Koutsoyiannis, L. Brandimarte, and G. Blöschl, "Flood fatalities in Africa: from diagnosis to mitigation," *Geophysical Research Letters*, vol. 37, no. 22, 2010.
- [19] P. Vogel, P. Knippertz, A. H. Fink, A. Schlueter, and T. Gneiting, "Skill of global raw and postprocessed ensemble predictions of rainfall over northern tropical Africa," *Weather and Forecasting*, vol. 33, no. 2, pp. 369–388, 2018.
- [20] S. Kolios and H. Feidas, "An automated nowcasting system of mesoscale convective systems for the Mediterranean basin using Meteosat imagery. Part I: system description," *Meteorological Applications*, vol. 20, no. 3, pp. 287–295, 2013.
- [21] K. Peters, C. Hohenegger, and D. Klocke, "Different representation of mesoscale convective systems in convection-permitting and convection-parameterizing NWP models and its implications for large-scale forecast evolution," *Atmosphere*, vol. 10, no. 9, Article ID 503, 2019.
- [22] A. G. Laing, R. Carbone, and V. Levizzani, "Cycles and propagation of deep convection over equatorial Africa," *Monthly Weather Review*, vol. 139, pp. 2832–2853, 2011.
- [23] Z. Feng, L. R. Leung, S. Hagos, R. A. Houze, C. D. Burleyson, and K. Balaguru, "More frequent intense and long-lived storms dominate the springtime trend in central US rainfall," *Nature Communications*, vol. 7, Article ID 13429, 2016.
- [24] M. Maranan, A. H. Fink, P. Knippertz et al., "Interactions between convection and a moist vortex associated with an extreme rainfall event over southern West Africa," *Monthly Weather Review*, vol. 147, no. 7, pp. 2309–2328, 2019.
- [25] B. Jackson, S. E. Nicholson, and D. Klotter, "Mesoscale convective systems over western equatorial Africa and their relationship to large-scale circulation," *Monthly Weather Review*, vol. 137, no. 4, pp. 1272–1294, 2009.
- [26] J. P. Grist and S. E. Nicholson, "A study of the dynamic factors influencing the interannual variability of rainfall in the West African Sahel," *Journal of Climate*, vol. 14, pp. 1337–1359, 2001.
- [27] R. S. Tanessong, D. A. Vondou, Z. Y. Djomou, and P. M. Igri, "WRF high resolution simulation of an extreme rainfall event over Douala (Cameroon): a case study," *Modeling Earth Systems and Environment*, vol. 3, no. 3, pp. 927–942, 2017.
- [28] P. M. Igri, R. S. Tanessong, D. A. Vondou et al., "Assessing the performance of WRF model in predicting high-impact weather conditions over Central and Western Africa: an ensemble-based approach," *Natural Hazards*, vol. 93, no. 3, pp. 1565–1587, 2018.
- [29] J. B. Suchel, *Les regions climatiques du Cameroun. Les climats du Cameroun*, Ph.D. thesis vol. 4, Université St Étienne (France), , 1987.
- [30] D. Sighomnou, *Analyse et redéfinition des régimes climatiques et hydrologiques du Cameroun: perspectives d'évolution des ressources en eau*, Ph.D. thesis, Université de Yaoundé I, Yaoundé, 2004.
- [31] S. W. Nesbitt and E. J. Zipser, "The diurnal cycle of rainfall and convective intensity according to three years of TRMM measurements," *Journal of Climate*, vol. 16, no. 10, pp. 1456–1475, 2003.
- [32] A. Creese and R. Washington, "Using qflux to constrain modeled Congo Basin rainfall in the CMIP5 ensemble," *Journal of Geophysical Research: Atmospheres*, vol. 121, no. 22, pp. 13,415–13,442, 2016.
- [33] S. E. Nicholson, "The ITCZ and the seasonal cycle over equatorial Africa," *Bulletin of the American Meteorological Society*, vol. 99, no. 2, pp. 337–348, 2018.

- [34] H. Wu, X. Xu, T. Luo, Y. Yang, Z. Xiong, and Y. Wang, "Variation and comparison of cloud cover in MODIS and four reanalysis datasets of ERA-interim, ERA5, MERRA-2 and NCEP," *Atmospheric Research*, vol. 281, Article ID 106477, 2023.
- [35] A. Dommo, D. A. Vondou, N. Philippon, R. Eastman, V. Moron, and N. Aloysius, "The ERA5's diurnal cycle of low-level clouds over Western Central Africa during June–September: dynamic and thermodynamic processes," *Atmospheric Research*, vol. 280, Article ID 106426, 2022.
- [36] H. Hersbach, B. Bell, P. Berrisford et al., "The ERA5 global reanalysis," *Quarterly Journal of the Royal Meteorological Society*, vol. 146, no. 730, pp. 1999–2049, 2020.
- [37] T. Fiolleau, "Cycle de vie des systèmes convectifs de mousson dans les régions tropicales: préparation à la mission Megha-Tropiques," *Climatologie. Ecole Polytechnique X, Français*. Pastel-00576870, 2010.
- [38] C. Morel and S. Senesi, "A climatology of mesoscale convective systems over Europe using satellite infrared imagery. I: methodology," *Quarterly Journal of the Royal Meteorological Society*, vol. 128, no. 584, pp. 1953–1971, 2022.
- [39] D. A. Vondou, A. Nzeukou, and F. M. Kamga, "Diurnal cycle of convective activity over the west of Central Africa based on Meteosat images," *International Journal of Applied Earth Observation and Geoinformation*, vol. 12, pp. S58–S62, 2010.
- [40] T. Fiolleau and R. Roca, "An algorithm for the detection and tracking of tropical mesoscale convective systems using infrared images from geostationary satellite," *IEEE Transactions on Geoscience and Remote Sensing*, vol. 51, no. 7, pp. 4302–4315, 2013.
- [41] X. Huang, C. Hu, X. Huang et al., "A long-term tropical mesoscale convective systems dataset based on a novel objective automatic tracking algorithm," *Climate Dynamics*, vol. 51, no. 7–8, pp. 3145–3159, 2018.
- [42] V. Patil, S. Das, and A. Phadke, "Methods for mesoscale convective systems detection and tracking: a survey," in *2019 10th International Conference on Computing, Communication and Networking Technologies (ICCCNT)*, pp. 1–7, IEEE, Kanpur, India, 2019, July.
- [43] J. Kukulies, D. Chen, and M. Wang, "Temporal and spatial variations of convection, clouds and precipitation over the Tibetan Plateau from recent satellite observations. Part II: precipitation climatology derived from global precipitation measurement mission," *International Journal of Climatology*, vol. 40, no. 11, pp. 4858–4875, 2020.
- [44] D. R. Dowling and L. F. Radke, "A summary of the physical properties of cirrus clouds," *Journal of Applied Meteorology and Climatology*, vol. 29, no. 9, pp. 970–978, 1990.
- [45] K. N. Liou, "Influence of cirrus clouds on weather and climate processes: a global perspective," *Monthly Weather Review*, vol. 114, no. 6, pp. 1167–1199, 1986.
- [46] K. Sassen, Z. Wang, and D. Liu, "Cirrus clouds and deep convection in the tropics: Insights from CALIPSO and CloudSat," *Journal of Geophysical Research: Atmospheres*, vol. 114, no. D4, 2009.
- [47] C. M. Dunning, E. C. L. Black, and R. P. Allan, "The onset and cessation of seasonal rainfall over Africa," *Journal of Geophysical Research: Atmospheres*, vol. 121, no. 19, pp. 11,405–11,424, 2016.
- [48] B. Liebmann, I. Bladé, G. N. Kiladis et al., "Seasonality of African precipitation from 1996 to 2009," *Journal of Climate*, vol. 25, no. 12, pp. 4304–4322, 2012.
- [49] H. Hu, L. R. Leung, and Z. Feng, "Observed warm-season characteristics of MCS and non-MCS rainfall and their recent changes in the Central United States," *Geophysical Research Letters*, vol. 47, no. 6, Article ID e2019GL086783, 2020.
- [50] R. S. Schumacher and K. L. Rasmussen, "The formation, character and changing nature of mesoscale convective systems," *Nature Reviews Earth & Environment*, vol. 1, no. 6, pp. 300–314, 2020.
- [51] T. Becker, P. Bechtold, and I. Sandu, "Characteristics of convective precipitation over tropical Africa in storm-resolving global simulations," *Quarterly Journal of the Royal Meteorological Society*, vol. 147, no. 741, pp. 4388–4407, 2021.
- [52] B. Feng, Y. Zhang, and R. Bourke, "Urbanization impacts on flood risks based on urban growth data and coupled flood models," *Natural Hazards*, vol. 106, no. 1, pp. 613–627, 2021.
- [53] R. Wang, T. Xian, M. Wang et al., "Relationship between extreme precipitation and temperature in two different regions: the Tibetan Plateau and Middle-East China," *Journal of Meteorological Research*, vol. 33, no. 5, pp. 870–884, 2019.
- [54] Z. Yong, J. Xiong, Z. Wang, W. Cheng, J. Yang, and Q. Pang, "Relationship of extreme precipitation, surface air temperature, and dew point temperature across the Tibetan Plateau," *Climatic Change*, vol. 165, Article ID 41, 2021.
- [55] G. Kuete, W. Pokam Mba, and R. Washington, "African Easterly Jet South: control, maintenance mechanisms and link with Southern subtropical waves," *Climate Dynamics*, vol. 54, pp. 1539–1552, 2020.
- [56] W. M. Pokam, L. A. T. Djotang, and F. K. Mkankam, "Atmospheric water vapour transport and recycling in equatorial central africa through NCEP/NCAR reanalysis data," *Climate Dynamics*, vol. 38, no. 9–10, pp. 1715–1729, 2012.
- [57] D. A. Vondou, G. M. Guenang, T. L. Djotang, and P. Honore, "Trends and interannual variability of extreme rainfall indices over cameroon," *Sustainability*, vol. 13, no. 12, Article ID 6803, 2021.
- [58] S. E. Nicholson and J. P. Grist, "The seasonal evolution of the atmospheric circulation over West Africa and equatorial Africa," *Journal of Climate*, vol. 16, no. 7, pp. 1013–1030, 2003.
- [59] E. L. E. Dyer, D. B. A. Jones, J. Nusbaumer et al., "Congo Basin precipitation: assessing seasonality, regional interactions, and sources of moisture," *Journal of Geophysical Research: Atmospheres*, vol. 122, no. 13, pp. 6882–6898, 2017.
- [60] F. Song, G. J. Zhang, V. Ramanathan, and L. R. Leung, "Trends in surface equivalent potential temperature: a more comprehensive metric for global warming and weather extremes," *Proceedings of the National Academy of Sciences*, vol. 119, no. 6, Article ID e2117832119, 2022.
- [61] N. C. Privé and R. A. Plumb, "Monsoon dynamics with interactive forcing. Part I: axisymmetric studies," *Journal of the Atmospheric Sciences*, vol. 64, no. 5, pp. 1417–1430, 2007.
- [62] J. Nie, W. R. Boos, and Z. Kuang, "Observational evaluation of a convective quasi-equilibrium view of monsoons," *Journal of Climate*, vol. 23, no. 16, pp. 4416–4428, 2010.
- [63] A. Arakawa and W. H. Schubert, "Interaction of a cumulus cloud ensemble with the large-scale environment, Part I," *Journal of the Atmospheric Sciences*, vol. 31, no. 3, pp. 674–701, 1974.
- [64] G. J. Zhang and N. A. McFarlane, "Sensitivity of climate simulations to the parameterization of cumulus convection in the Canadian climate centre general circulation model," *Atmosphere-Ocean*, vol. 33, no. 3, pp. 407–446, 1995.
- [65] C. Fritz, Z. Wang, S. W. Nesbitt, and T. J. Dunkerton, "Vertical structure and contribution of different types of precipitation during Atlantic tropical cyclone formation as

- revealed by TRMM PR,” *Geophysical Research Letters*, vol. 43, no. 2, pp. 894–901, 2016.
- [66] W. Xu, H. Chen, H. Wei, Y. Luo, and T. Zhao, “Extreme precipitation produced by relatively weak convective systems in the tropics and subtropics,” *Geophysical Research Letters*, vol. 49, no. 7, Article ID e2022GL098048, 2022.
  - [67] A. Hamada, Y. N. Takayabu, C. Liu, and E. J. Zipser, “Weak linkage between the heaviest rainfall and tallest storms,” *Nature Communications*, vol. 6, Article ID 6213, 2015.
  - [68] E. J. Zipser and C. Liu, “Extreme convection vs. Extreme rainfall: a global view,” *Current Climate Change Reports*, vol. 7, pp. 121–130, 2021.
  - [69] S. Shige, S. Kida, H. Ashiwake, T. Kubota, and K. Aonashi, “Improvement of TMI rain retrievals in mountainous areas,” *Journal of Applied Meteorology and Climatology*, vol. 52, no. 1, pp. 242–254, 2013.
  - [70] M. K. Yamamoto, S. Shige, C.-K. Yu, and L.-W. Cheng, “Further improvement of the heavy orographic rainfall retrievals in the GSMaP algorithm for microwave radiometers,” *Journal of Applied Meteorology and Climatology*, vol. 56, no. 9, pp. 2607–2619, 2017.
  - [71] L. W. Uccellini and D. R. Johnson, “The coupling of the upper and lower tropospheric jet streaks and implications for the development of convective storms,” *Monthly Weather Review*, vol. 107, no. 6, pp. 682–703, 1979.
  - [72] E. J. Zipser, D. J. Cecil, C. Liu, S. W. Nesbitt, and D. P. Yorty, “Where are the most intense thunderstorms on earth?” *Bulletin of the American Meteorological Society*, vol. 87, no. 8, pp. 1057–1072, 2006.